Article

Understanding API Static Drying with Hot Gas Flow: Design and Test of a Drying Rig Prototype and Drying Modeling Development

Sara Ottoboni,* Simon J. Coleman, Christopher Steven, Mariam Siddique, Marine Fraissinet, Marion Joannes, Audrey Laux, Alastair Barton, Paul Firth, Chris J. Price, and Paul A. Mulheran

Cite This: *Org. Process Res. Dev.* 2020, 24, 2505−2520

Read Online

ACCESS | Metrics & More | Article Recommendations | Supporting Information

ABSTRACT: Developing a continuous isolation process to produce a pure, dry, free-flowing active pharmaceutical ingredient (API) is the final barrier to the implementation of continuous end-to-end pharmaceutical manufacturing. Recent work has led to the development of continuous filtration and washing prototypes for pharmaceutical process development and small-scale manufacture. Here, we address the challenge of static drying of a solvent-wet crystalline API in a fixed bed to facilitate the design of a continuous filter dryer for pharmaceutical development, without excessive particle breakage or the formation of interparticle bridges leading to lump formation. We demonstrate the feasibility of drying small batches on a time scale suitable for continuous manufacturing, complemented by the development of a drying model that provides a design tool for process development. We also evaluate the impact of alternative washing and drying approaches on particle agglomeration. We conclude that our approach yields effective technology, with a performance that is amenable to predictive modeling.

KEYWORDS: *pharmaceutical, drying, agglomeration, modeling, model validation*

1. INTRODUCTION

The vast majority of small-molecule pharmaceutical materials are isolated by crystallization, followed by filtration, washing, and drying. Although particle design by crystallization has been the subject of intensive research effort over the last 2 decades, there has been less focus on the role of filtration, washing, and drying in defining particle attributes. This gap is especially significant in the area of continuous pharmaceutical manufacturing where the lack of small-scale equipment for process development and small-scale cGMP manufacturing is a barrier to the implementation of end-to-end continuous drug substance manufacturing.[1]

The goal of particle engineering is to generate crystalline active pharmaceutical ingredient (API) particles which are chemically and phase pure (i.e., the desired polymorph) with a particle size distribution (PSD), which is appropriate for the intended formulation. This must be accomplished while keeping the impurities of synthesis, any unreacted starting materials and byproducts, in solution while minimizing the solvent usage and processing time. The particle suspension generated in this way is the starting point for the development of filtration, washing, and drying steps, which strive to deliver the product as pure free-flowing particles ready for formulation. Dead end filtration provides a mechanism by which the bulk of the crystallization mother liquor is removed along with the associated impurities. The best practice is to halt the filtration while the cake is still fully saturated, that is, to stop at the point where the filter cake surface is just exposed (this is frequently referred to as "dryland").[2] The simplest choice of wash solvent is the crystallization solvent (or solvent mixture) chilled to the end point temperature of the crystallization to minimize product loss by dissolution during the passage of the wash solvent through the filter cake. The

quantity of wash solvent may be subject to optimization, a typical starting quantity would be 1 cake volume, providing a suitable overage relative to the one cake void volume of mother liquor remaining in the saturated filter cake.[3] Typically, the next process step might be to displace the first wash solvent by washing with a different solvent selected to be miscible with the crystallization solvent but one in which the API has rather low solubility. This practice is chosen to balance the combined objectives of displacing the impurity-laden mother liquor to deliver chemically pure API and removing the wash solvent to leave the API wet in a solvent, which is less likely to promote the formation of lumps on drying.[4]

This paper focuses on the role of drying and is written on the supposition that the filtration and washing steps described above have been accomplished successfully to leave a wet filter cake damp with predominantly a wash solvent with a small trace of the crystallization solvent remaining. At first sight, this drying task may appear straightforward; however, there are several processing requirements which must be understood and met.

First, the product should be dry, at least to the extent that the quantity of each solvent remaining in the isolated product is well below the limit for that solvent calculated using the ICH Q3 guidance, which takes account of the anticipated patient exposure based on the drug substance dose and the quantity of solvent the isolated drug substance contains.[5]

The second requirement is that the process of drying should not lead to the formation of lumps in the final product powder discharged from the dryer.[6] This can arise easily if the API has any solubility in the residual solvent, be it the final traces of crystallization solvent(s) or the wash solvent(s).[7] In practice, this may pose some difficulties; by definition of being appropriate as a crystallization solvent, the API must have some modest solubility in the crystallization solvent at the isolation temperature/composition. Displacing this by washing with a nonsolvent is problematic because if the two solvents are miscible, the washing solvent is likely to behave as an antisolvent and drive dissolved API out of the solution during washing, thus forming lumps in the damp filter cake. If the nonsolvent is immiscible with the primary solvent, then the washing efficiency is likely to be low and the washed filter cake is likely to contain domains of particles which remain wet in the initial crystallization solvent which may promote lump formation during drying.[8] To avoid these issues arising from the use of true nonsolvents, solvents where the API solubility is very low may be used, but the evaporation of these solvents will still tend to result in lump formation, whose strength is strongly influenced by the mass of the crystalline material deposited during drying.

It is also important to consider the role of the product particles in the filter cake transporting solvent from the bulk to the cake surface where evaporation takes place. This process of solvent-mediated transport of dissolved species is in some ways analogous to chromatography, though driven by surface evaporation, which serves to concentrate the dissolved material at the surface of the dry cake. The resulting solid deposition tends to produce a product with a fused surface and a softer core if there is no agitation during drying.[9] Chemical impurities remaining in solution in the solvent removed during drying are also transported to the drying surface where they are concentrated. If these impurities are highly colored, this effect is visually striking and the inhomogeneous distribution of impurities is readily apparent and the material is likely to be subject to rework at the least.[4] However, if both the product and impurities form white powders, there is no visual evidence of inhomogeneity and the risk of local impurities exceeding the assay limit is real. For this reason, some form of powder blending is routinely undertaken to mitigate against the risk of nonrepresentative sampling.

Another important aspect to consider is the role of cake cracking during drying. Inevitably, as a solvent is removed from the filter cake dried without agitation, there will be either some tendency for shrinkage or cake cracking or both of which will result in some preferential flow paths for the drying gas (typically a heated gas, possibly air in small-scale laboratory experiments or nitrogen at larger scale to mitigate the flammability risk). Cracking of the cake will reduce the efficiency of drying as part of the gas flow will not then fully release the heat energy it carries or pick up as much solvent vapor as it would otherwise.

The drying process requires a heat input to balance the energy removed due to the latent heat of evaporation of the solvent removed during drying. If no heat is provided, the filter cake will cool down, and the rate of drying will decline because of the reduced solvent vapor pressure at lower temperatures. Tracking drying gas temperature provides a simple practical method to track the progress of drying. If no heat is provided, the filter cake will become very cold and if exposed to moist air either a drying gas (rare in pharmaceutical practice) or on powder discharge, there is the potential for condensation of water which will impact product quality.[10]

2. AIMS

The research objective of this work was to investigate drying of solvent-wet pharmaceutical materials in a fixed bed formed as a small diameter filter cake as a part of the process to design a continuous filter dryer for pharmaceutical development and small-scale continuous manufacturing. The key research questions focus on determining the feasibility of delivering sufficient energy to evaporate residual organic solvent using a combination of reduced outlet pressure and flowing heated nitrogen. An associated objective was to determine the impact of drying on particle agglomeration and in particular to investigate the effect of different washing and drying approaches. A drying model was also designed to allow different drying approaches to be simulated to facilitate the design process based on reliable prediction of dryer performance.

3. MATERIALS AND METHODS

3.1. Materials for Prototyping Test and Experiments with the API. The solid material used for the model validation experiments was sodium bicarbonate, supplied by Tata Chemicals Europe, Medium Granular, 99.3% purity. x_{50} = 158.43 μm, Sauter mean diameter (SMD) = 148.51 μm. The wash solvent used for the sodium bicarbonate experiments was deionized water saturated with sodium bicarbonate. The solubility of sodium bicarbonate in water at 20 °C is 0.096 g/g water. The drying kinetics are slower using a saturated water solution compared to a more conventional organic wash solvent [e.g., isopropanol (IPA)], thereby allowing the differences in drying rate to be captured for each experiment. The drying gas used for these experiments was air.

3.2. Materials for Prototyping Test and Experiments with the API. A series of different compounds were used to verify the drying model and to test the drying rig prototype. Potassium hydrogen L-tartrate was supplied by Alfa Aesar (batch number 10202036, purity 98+%) and three different grades of paracetamol were used. Micronized, powder, and special granular pharmaceutical grade paracetamol ($C_8H_9NO_2$) was supplied by Mallinckrodt Inc., Raleigh, N.C., USA. Micronized (batch number 042213E407), powder (batch number 637514D001), and granular (batch number 161713J561) paracetamol was used throughout the work reported here. Sodium bicarbonate and potassium hydrogen L-tartrate were selected because of their nontoxicity and the possibility to test the drying rig outside the fume hood (in Alconbury Weston's manufacturing facility) before the commissioning in the University of Strathclyde laboratories and for their similar PSD to the paracetamol grades used (potassium hydrogen L-tartrate x_{50}, 57 μm and SMD, 41 μm). Paracetamol was selected as the active pharmaceutical test compound. Paracetamol shows oral toxicity and skin and eye irritation risks and it is considered to be a skin sensitizer. The basis for selecting the three grades of paracetamol is that the micronized material is challenging to filter, wash, and dry because of its small particle size and it also has an increased agglomeration propensity because of its small size, leading to difficulty in removing the mother liquor during washing; it shows wide size distribution and damaged particle surfaces. The powder represents a typical API and the special granular material poses a challenge because of its large particle size. These three grades represent the typical range of particle sizes used in the pharmaceutical industry (micronized paracetamol, x_{50}, 24.55 μm, SMD, 18.66 μm; powder paracetamol, x_{50}, 64.03 μm, SMD, 46.35 μm; and granular paracetamol, x_{50},
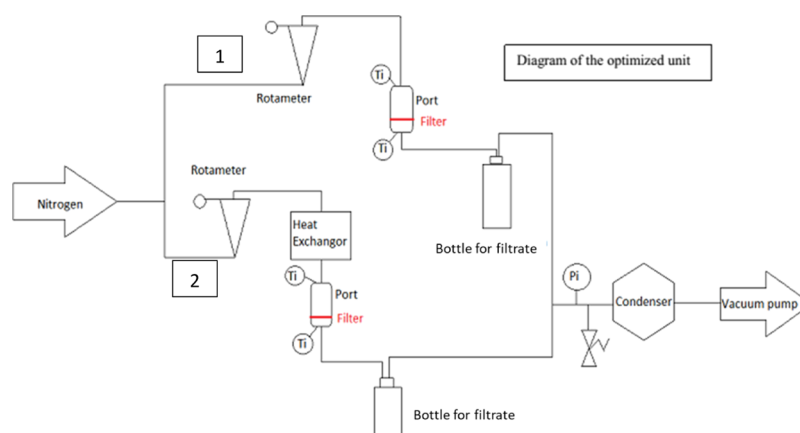
Figure 1. Schematic representation of the drying rig prototype.

363.58 μm, SMD, 299.30 μm). The PSD and bulk density of these paracetamol grades are reported in the Supporting Information section.

The crystallization solvents selected for this study were Millipure water (Milli-Q, Germany; water temperature = 23.2 °C, TOC = 2 ppb) that was selected as a crystallization and wash solvent for the potassium hydrogen L-tartrate for its relatively low aqueous solubility (0.006 g/g of water)[11] and as a paracetamol crystallization solvent for its relatively low solubility (0.013 g/g at 25 °C, measured by the gravimetric method). Water as the crystallization solvent for paracetamol is widely used, even though the solubility is relatively low and there are difficulties related to poor wetting. To address these two problems with water, ethanol was also used as the crystallization solvent for paracetamol [purity ≥99.8% (gas chromatography (GC), Sigma-Aldrich]. Ethanol was selected for its low toxicity and higher capability to dissolve paracetamol (0.206 g/g at 25 °C, measured by the gravimetric method).

To remove the residual mother liquor remaining in the cake after the filtration process, the cakes were washed. Millipure water was selected as a washing solution for potassium hydrogen L-tartrate cakes. n-Heptane (purity 99%, Alfa Aesar), IPA [purity ≥99.5% (GC), Sigma-Aldrich], and n-dodecane (purity 99%, Alfa Aesar) were used for paracetamol cakes. n-Heptane and n-dodecane were selected for their very low paracetamol solubility (n-heptane, 0.0001 g/g and n-dodecane 0.0007 g/g at 25 °C, measured by gravimetric method[9]) and for their capability to displace the mother liquor from the cake. n-Heptane shows miscibility with ethanol while n-dodecane does not; the miscibility improves washing efficiency, allowing washing by displacement, diffusion, and dilution of the residual mother liquor. IPA was selected as a wash solvent because of the slightly higher paracetamol solubility (0.109 g/g at 25 °C, measured by gravimetric method[9]) to promote agglomeration during drying.

Ethanol, IPA, n-heptane, and n-dodecane are flammable solvents. Ethanol and IPA cause eye irritation. IPA has specific target organ toxicity (in single exposure). n-Heptane causes skin irritation and chronic aquatic toxicity and it has specific target organ toxicity (in single exposure) and aspiration hazard. n-Dodecane also shows aspiration toxicity.

4. METHODS

4.1. Drying Rig. A commercial continuous isolation platform able to process—in a flexible way—small quantities of APIs to reduce the API required for isolation development in

R&D has been prototyped in collaboration with Alconbury Weston Ltd. This serves to reduce the amount of material consumed in order to define the isolation strategy of a new chemical entity underdevelopment in the pharmaceutical industry. This continuous filtration and drying unit was developed during the Remedies project (App B)[4] and has been named CFD20. The CFD20 unit allows filtration, followed by up to three washing steps with two different solvents, deliquoring, and then drying.[12] A full description of the AWL continuous filter drier (CFD) is described in a previous paper by the authors.[9]

The Unit Consists of

- A slurry tank where the slurry is mixed by an agitator to allow homogeneous slurry mixing.
- A vacuum system used to transfer the slurry to the isolation carousel. The carousel is made of 10 different positions where filtration, multiple washing stages, deliquoring, and drying are carried out. Each position consists of a 90 mL glass cylinder positioned on top of a metal sintered 20 μm mesh BOPP filter (G. Bopp & Co. AG). Position 1 of the carousel is used for slurry feeding and filtration, positions 2 and 3 can be used for multiple washing steps, position 4 can be used for additional washing if required and for deliquoring, while positions 5–9 are used for drying. In position 10, there is no filter media in the base to allow the dried cake removal by using a piston that mechanically ejects the dry cake.
- Two wash solvent containers connect to the washing positions. To prevent disturbance of the filter cake surface, the wash solvent is dispensed on top of the cake using a solvent atomizer.
- An innovative vision system is used for fine control over the filtration and washing. A camera monitors liquid levels and cake heights to automatically stop filtration just before dryland to prevent cake cracking and to accurately dispense and drain wash solvents for efficient washing and reducing solvent waste.
- A receiver is used to collect the liquid phase removed to analyze the impurity content in each filtrate phase offline. This is connected to the bottom of each carousel position.

Static drying is carried out by drawing a vacuum through the receiver container beneath the port and the inlet of the drying gas above the port at a positive pressure, allowing a flow of air/nitrogen to flow through the cake. The temperature of the inlet gas is controlled by an electrically heated transfer line.

To improve the drying capability of CFD20 and to drive further improvements, which have been embodied in the subsequent CFD unit (AWL CFD25), a fast prototyping approach was followed to design and build the drying rig prototype created to study the CFD25 drying components.[13]

The drying rig scheme is shown in Figure 1. The system can simultaneously dry four cakes placed in four different ports, with inner diameters of 20 mm; however, to maximize the drying rate, two drying ports can be used simultaneously. The nitrogen coming from the gas cylinder flows in two different paths (1 and 2): path 1 is used to dry the cake at room temperature and path 2 used to dry the cake using heated nitrogen. In each line, the nitrogen flow is controlled using two separate rotameters. The nitrogen flows in the rotameter of path 1 and then flows through the drying port where the cake is located. To monitor the drying temperature, probes are connected to the top of the port and below the sintered metal 20 μm filter media (BOPP). The temperature measured at the top of the port and the temperature measured below the filter media will be referred to as the inlet temperature and the outlet temperature, respectively, throughout the paper. A third probe was used during the prototype development to measure the cake temperature during drying. As reported in Figure 1, the third probe was removed from the final drying rig because it was causing inconsistent drying results, probably because of the disturbance of the cake. The temperature probes are connected to a human–machine interface (HMI), which also provided data logging. In addition, the pressure sensor connected to the lid of the filtration bottles is also logged. The solvent removed during drying is collected in a bottle maintained at reduced pressure to facilitate solvent evaporation. In path 2, the nitrogen coming out from the rotameter is heated using a copper coil of length 13.5 m with a diameter of 3 mm submerged in a water bath. The water bath temperature was set to a maximum of 75 °C, using a nitrogen flow of 15.5 L/min and a nitrogen pressure of 0.4 bar (from the gas cylinder), and the maximum temperature reached in the port was measured to be 54.5 °C. To maintain the nitrogen temperature and avoid heat loss, the tubing of path 2 is thermally insulated (as can be seen in Figures 1 and 2).

The flow of drying gas (15.5 L/min) relative to the mass of the cake (approximately 10 g) is rather large in this study, higher than that typically used in batch-agitated Nutsche filter dryers. However, the AWL CFD processes small cake volumes in a semicontinuous manner, which allows for a significantly lower residence time for drying (typically 5 to 10 min). This high gas flow enables the cycle time to be reduced, thereby increasing the throughput on a relatively small platform.

As can be seen in Figure 2, the two ports are supported by a metallic stand where they are connected to the waste solvent bottles (bottles of filtrate). To seal the ports during drying, a polypropylene lid holding the temperature probe is positioned on top and sealed with a Viton O-ring. The polypropylene base connected to the metallic stand holds the filter medium and is also sealed with a Viton O-ring. This arrangement allows the operator to perform cake filtration and washing in the same port before commencing drying. To facilitate port removal to measure the mass of the cake (with a two-digit scale) during drying, the top of the port can be easily removed and the bottom temperature probe can be unplugged from the HMI.

4.2. Drying Model. We developed a model for the drying of the cake under the simplifying assumption that it dries evenly throughout the process with a uniform temperature and solvent content that changes over time. This allows a straightforward
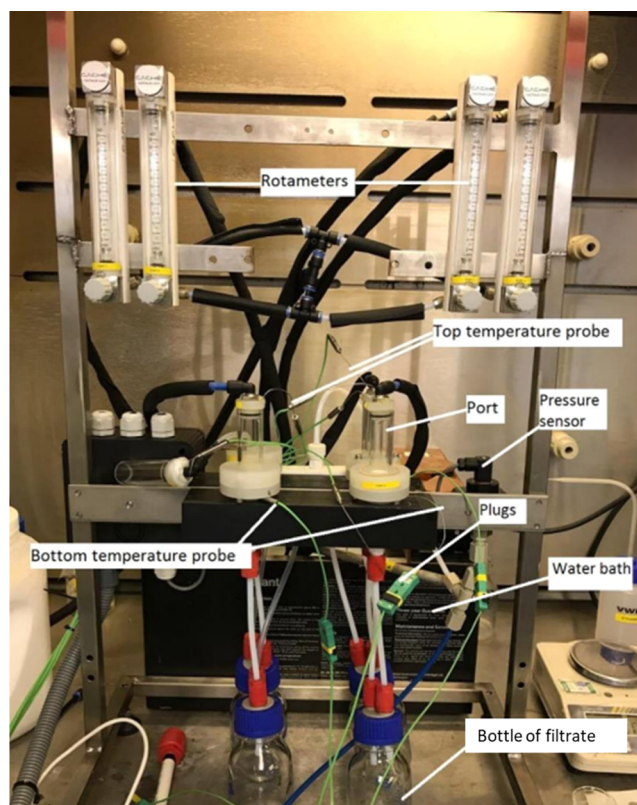

Figure 2. Image of the drying rig.

differential energy and mass balance to be applied to the cake as a whole, and to the drying gas stream on exiting the cake, yielding predictions for the drying rate over time. The model assumes that the gas flow rate through the cake is known, along with the pressures above and below the cake and the inlet gas temperature. We also assume that the gas flow induces evaporative drying only and do not attempt to predict the initial mechanical blow-through of moisture when the gas stream is first started.

We start by applying the ideal gas law to the inlet gas stream because this is a very good approximation to real gasses used in this work:

$$P_{in} \times \dot{V}_{in} = F_d \times R \times T_{in} \tag{M1}$$

Here, P_{in}, T_{in}, and $\dot{V}_{in}$ are the pressure, temperature, and volumetric flow rate of the inlet gas stream, R is the universal gas constant, and F_d is the molar flow rate of this drying gas stream. The latter is used to calculate the volumetric flow rate of the gas leaving the cake, when it has acquired some of the solvent as vapor.

We will assume that the exiting gas will reach a fraction f of full saturation and treat this as a free parameter in the results we present below. Using M1, we find

$$\dot{V}_{out}(t) = \frac{T_s(t)}{T_{in}} \frac{P_{in}}{(P_{out} - f \times P_s(T_s(t)))} \dot{V}_{in} \tag{M2}$$

where $\dot{V}_{out}(t)$ is the time-dependent volumetric flow rate of the gas leaving the cake. We assume that the exiting gas stream, the cake particles, and solvent are in thermal equilibrium, so that $T_s(t)$ is the temperature of the cake, solvent, and exiting gas at time t. Note that we take account of the partial pressure of the drying gas in performing the mass balance in M2. $T_s(t)$ is the

temperature of the cake and its solvent that can also vary with time, P_{out} is the known pressure of the outlet stream, and $P_s(T_s(t))$ is the saturation pressure of the solvent at temperature $T_s(t)$.

The volumetric flow rate leaving the cake carries the solvent vapor and hence determines the rate of mass loss:

$$\frac{d}{dt}M(t) = -\dot{V}_{out}(t) \times \frac{f \times P_s(T_s)}{R \times T_s(t)} \times m_s \tag{M3}$$

where $M(t)$ is the mass of solvent in the cake and m_s is the molecular weight of the solvent.

In order to complete the model definition, we need to consider the differential energy balance that determines the evolution of the cake temperature. The total sensible heat change of the cake is related to its temperature change by

$$[M_p \times c_p + M(t) \times c_s] \times \frac{d}{dt}T_s(t) = \dot{Q}_d + \dot{Q}_e + \dot{Q}_{evap} \tag{M4}$$

Here, M_p is the dry particle mass of the cake, c_p and c_s are the heat capacities of the particles and solvent, respectively, and the heat flows on the right are defined below.

The rate of sensible heat gained by the sample due to the loss from the drying gas stream is given by

$$\dot{Q}_d = \frac{P_{in} \times \dot{V}_{in}(t)}{R \cdot T_{in}(t)} \times m_d \times c_d \times [T_{in} - T_s(t)] \tag{M5}$$

where m_d is the molecular weight of the drying gas and c_d is its heat capacity.

The rate of sensible heat gain by the sample from the environment is

$$\dot{Q}_e = U \times A \times [T_e - T_s(t)] \tag{M6}$$

where T_e is the external wall temperature, A is the effective area for heat transfer to the cake from the cylinder wall, and U is the overall heat-transfer coefficient.

An estimated value of $(U \times A)$, evaluated from the physical dimensions of the apparatus and a typical value of U at a water–solid interface, was used in the drying model to estimate the heat transfer through the glass walls of the drying rig ports. Preliminary experiments showed that a value of 0.2 was a reasonable estimation for this parameter.

Finally, the rate of heat loss from the sample due to evaporation is using M3

$$\dot{Q}_{evap} = \lambda \times \frac{d}{dt}M(t) \tag{M7}$$

where λ is the latent heat of vaporization of the solvent. Equations M2–M7 can be used to calculate the evolution of $M(t)$, the mass of solvent in the cake, and $T_s(t)$ is the temperature of the exiting gas stream, using the Euler method with time step 0.1 s.

4.3. Method for API Experiments. *4.3.1. Preliminary Material Characterization.* The solubility of paracetamol was measured in a series of solvents reported in the Materials and Methods section and determined by the isothermal equilibration and dry residue method.[9] Details are reported in the Supporting Information, along with solubility results and data for the solvents.

Particle size and size distribution were determined by using a Sympatec QICPIC particle size analyzer with a VIBRI/L setup at a feed pressure of 0.5 bar, a feed rate of 25%, and a 0.5 mm gap width. Agglomerated particles with a size smaller than 1 mm were analyzed in this way. Approximately 1 g of sample was used for the PSD characterization. The same methodology was used to analyze product PSD after drying. The size of the input material was then compared with the that of the samples of filtered, washed, and dried product to evaluate particle size and size distribution variations related to the isolation approach selected.

4.3.2. Slurry Preparation. The suspensions evaluated in this study were prepared by saturating the solvent with the selected compound (potassium L-tartrate, paracetamol, etc.). The quantity of compound required to saturate the solution was calculated from the solubility data. In case of paracetamol slurry, the solvent was saturated with paracetamol at 25 °C. In order to produce paracetamol suspensions with 10, 15, or 20% by volume of undissolved paracetamol, respectively, 3, 4.5, or 6 g of paracetamol was added to 20 g of saturated solution.

4.3.3. Filtration, Washing, and Drying Driven by the Drying Rig. The prepared slurry was transferred to a drying port. During filtration and washing, the port lid is removed. Vacuum is applied beneath the filter media (placed in the polypropylene bottom part of the port) to filter the cake to break through[a]. The solvent removed during filtration is collected in the filtration bottle. The cake was then washed gently by slowly running the wash down the wall of the filter tube using a disposable pipette. Great care was taken to minimize the disturbance of the filter cake surface and mixing of the clean wash liquor with the mother liquors in the cake. The wash solvent was then removed following the same procedure used to filter the cake.

Before starting the drying, the filtrate collection bottle is rinsed and dried and then reconnected to the drying rig. Cake mass is measured before the drying process. The drying duration for the design of experiment (DoE) experiments was 30 min. The drying process is paused after 5 and 15 min to record the cake mass, which is also measured at the end of drying.

4.3.4. Dried Sample Characterization. Residual solvent content, extent of agglomeration, and strength of the agglomerates formed were measured on the dried samples.[6] A detailed description of the methods used to measure the extent of agglomeration and the agglomerate brittleness index (ABI) are reported elsewhere.[9]

To estimate the residual solvent content after the drying, the samples were transferred to a sample vial and left for 24 h open to atmosphere to dry.

4.4. DoE Approach for API Experiments. A multivariate DoE approach was used to investigate the combined effects of slurry properties and process parameters on the quality of the final dried material. Factors selected for the DoE are solid loading, filtration pressure, number of washes, volume of wash solvent, and drying mechanism. MOODE Pro V11.0.1 (developed by MKS Umetrics[14]) was used to build a statistical model to identify how the selected responses can be correlated with the multivariate parameters. A linear D-optimal approach was used to reduce the number of experiments from 2048 (full factorial) to 19 experiments with three center points (and no constraint) used to determine the reproducibility of the experimental procedure. The design region designed by the software is a cubic region where cake mass, feed pressure, and wash solvent volume were selected as the axes.

The D-optimal approach is appropriate in this case because the experimental variables investigated comprise a combination of quantitative and qualitative factors.[15,16]

Table 1 comprises the list of variables, responses, and analytical techniques used to gather the selected responses.

Table 1. Factors and Responses for the DoE (Model Validation)

factors (abbreviation)	range
paracetamol grade (CDS)	micronized (M) and powder (F)
cake mass (*API)	3−6 g
nitrogen feed pressure (Pre)	200−400 mbar
volume of wash solvent (Vol)	5−10 mL
number of washes (Num)	1, 2
wash solvent (Was)	n-dodecane, IPA (2 propanol), n-heptane, ethanol
bath temperature (Bat)	25−75 °C

Responses (Abbreviation), Unit
*SMD (AP2), μm
*solvent content (LOD) after 30 min drying with drying rig (So2), %
driving force after 5 min drying (Dri), mbar
driving force after 15 min drying (Dri2), mbar
driving force after 30 min drying (Dri3), mbar
cake mass after 5 min drying (Ca2), g
cake mass after 15 min drying (Ca3), g
cake mass after 30 min drying (Ca4), g
*solvent content (LOD) after 30 min drying with drying rig + overnight in a vacuum oven (Fin), %
flow rate corrected after 5 min drying (Fl), L/min
flow rate corrected after 15 min drying (Fl2), L/min
flow rate corrected after 30 min drying (Fl3), L/min
*friability index, ABI index (Fr), -
*extent of agglomeration (% a), %
inlet temperature after 5 min drying (Top), °C
inlet temperature after 15 min drying (to2), °C
inlet temperature after 30 min drying (to3), °C
outlet temperature after 5 min drying (Bot), °C
outlet temperature after 15 min drying (Bo2), °C
outlet temperature after 30 min drying (Bo3), °C
cake mass before drying and after washing (Ca5), g
initial inlet temperature (Ini), °C
initial outlet temperature (In2), °C
heat transfer in gas (Hea), W
heat transfer in cake (He2), W
*mean delta T (top-bottom) (Mea), °C

The responses highlighted with * were used in the Results and Discussion section. The remaining responses were not included in the Results and Discussion section because the data collected show high measurement errors. For instance, the driving force is measured by subtracting from atmospheric pressure the absolute value of the vacuum applied and by adding the pressure of the nitrogen that is measured from the gas cylinder manometer (0.5 ± bar). On the other hand, cake mass and inlet and outlet temperature data were used to calculate the loss on drying (LOD) and the mean delta T values. Heat-transfer data were not considered in the Results and Discussion section because of the approximation made during the data estimation, related to the high measurement errors done to determine gas flow rate with the use of the flow meter (0.5 ± L/min).

4.5. Methods for Model Validation Experiments. The same drying kinetic rig described above was used to assess the accuracy of the drying model. Sodium bicarbonate was used as the solid material, deionized water saturated with sodium bicarbonate was used as the wash solvent, and compressed air was used as the drying gas. The effect of temperature, pressure, and cake height was investigated using the following values: the inlet gas temperature range was 25−45 °C, the pressure above the cake, controlled by a pressure regulator on the inlet of the system, was 0.25−2 bar, and the cake height was 20−50 mm. The results were compared with values predicted by the drying model.

The drying rig was altered slightly for these experiments, with the addition of pressure regulators and moisture trap on the compressed air inlet, and an electrically heated transfer line was used to heat the drying gas instead of the water bath heater. The components of the rig were set up in the following order: compressed nitrogen inlet, primary pressure regulator, moisture trap, secondary pressure regulator, rotameter, electrically heated transfer line, drying port with a filter plate, drying receiver vessel, pressure transmitter, and vacuum pump. The inlet temperature was measured at the top of the port. The outlet temperature was measured approximately 10 mm beneath the filter plate.

4.5.1. Sample Preparation. Each experiment was prepared by pouring the required mass of dry sodium bicarbonate into the port, recording cake height is achieved. A solution of deionized water saturated with sodium bicarbonate was then applied on top of the cake using a pipette so that the target starting moisture content of 25 wt % was achieved. The drying time was fixed at 10 min.
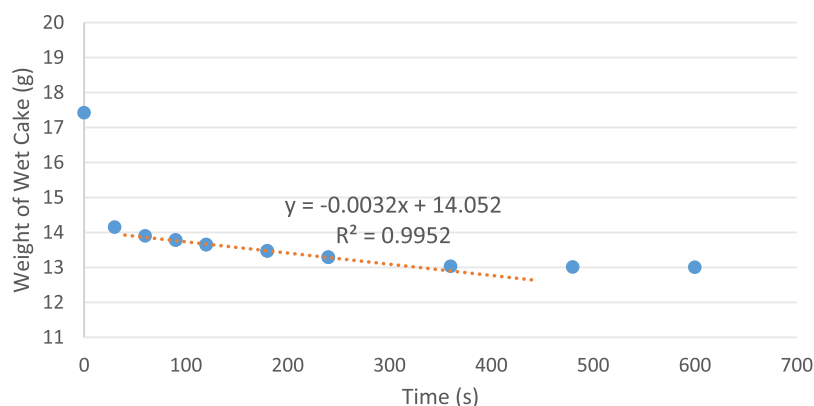

Figure 3. Weight of wet cake, measured intermittently during the drying process in the drying rig, illustrating the measurement of the drying rate during the constant drying rate period. Solid material = sodium bicarbonate; liquid = water saturated with sodium bicarbonate; height of cake = 35 mm; inlet temperature set point = 35 °C; and inlet pressure = 1 bar.
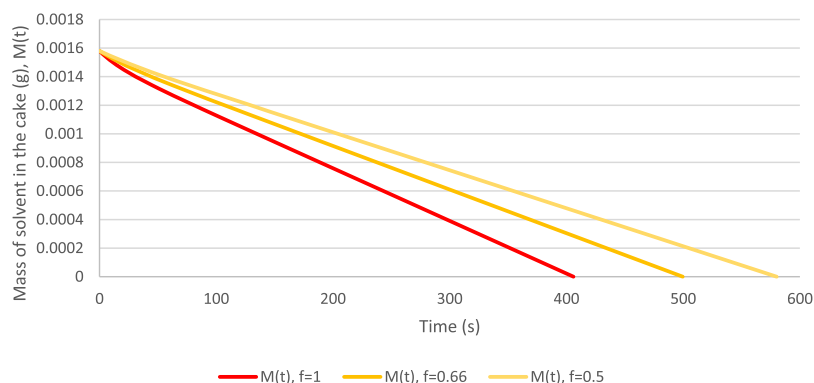
Figure 4. Drying model output, mass of solvent vs. time. Absolute pressure P_{in} = 1.25 bar(g), P_{out} = 0.45 bar(g), T_{in} = 45 °C, and cake height = 50 mm.
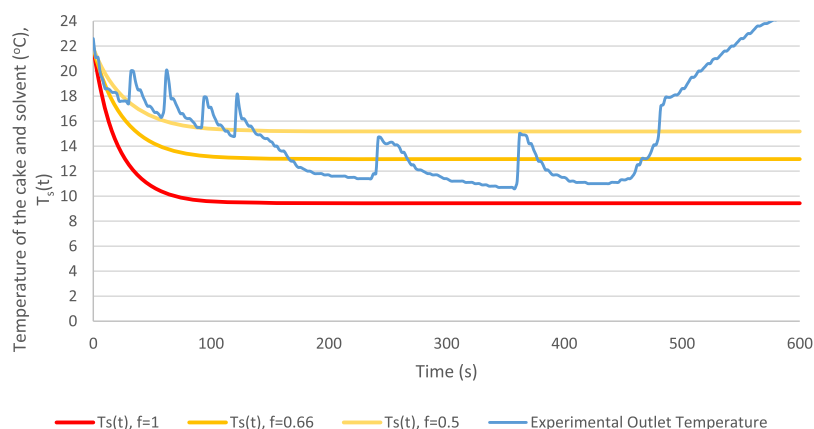

Figure 5. Drying model output, temperature of the cake and solvent P_{in} = 1.25 bar(g), P_{out} = 0.45 bar(g) (absolute pressure), T_{in} = 45 °C, and cake height = 50 mm. Blue line: Outlet temperature during drying experiment, P_{in} = 0.25 bar(g), T_{in} = 45 °C, and cake height = 50 mm.
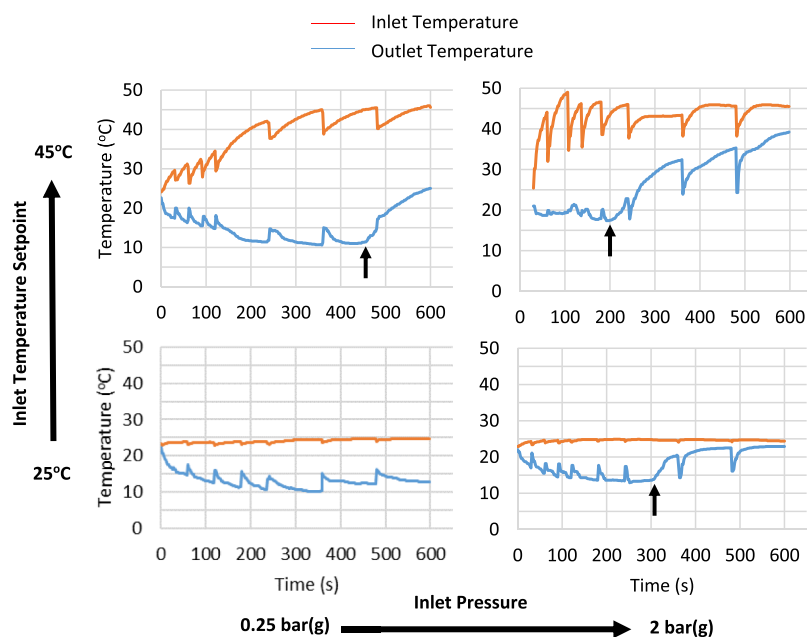

Figure 6. Temperature profiles for 50 mm cakes of sodium bicarbonate in water saturated with sodium bicarbonate. Red: inlet temperature. Blue: outlet temperature. Top left: temperature inlet set point = 45 °C; inlet pressure = 0.25 bar(g). Top right: temperature inlet set point = 45 °C; inlet pressure = 2 bar(g). Bottom left: temperature inlet set point = 25 °C; inlet pressure = 0.25 bar(g). Top left: temperature inlet set point = 45 °C; inlet pressure = 0.25 bar(g).

4.5.2. Dried Sample Characterization. The LOD was measured by placing the samples in an oven at 60 °C for at least 4 h and measuring the moisture content by weight. The extent of agglomeration was measured using a 1000 μm sieve and using gentle manual shaking by hand for 1 min before measuring the weight.

4.5.3. Measurement of Drying Rate. In order to gain reasonable comparisons of the rate of drying for each experimental run, it was paramount that the procedure for capturing and measuring the drying rate was consistent. The drying curve was captured by removing the port and recording its weight every 30 s, as shown in the example in Figure 3. Before measuring the weight, the bottom of the port was wiped to remove any droplets on the base.

For comparisons with the drying model, the constant drying rate period was examined. Figure 3 shows an example of the measurement of the drying rate of sodium bicarbonate particles in water. The initial drop in weight at the beginning of drying because of the mechanical removal of solvent can be clearly observed. The measurement of drying rate was therefore made after the first 30 s; this assumes that the majority of the moisture has already been removed mechanically. After the first 30 s, a line of regression was fitted up until the time when the decrease of the weight of the cake is no longer detectable, in this case around 360 s. It is assumed that almost all the solvent has been evaporated at this point. The drying rate can then be extracted using the gradient of the line of regression.

5. RESULTS AND DISCUSSION

5.1. Drying Model. Figures 4 and 5 show the examples of the outputs of the drying kinetic model for the case of $P_{in} = 0.25$ bar(g) and $T_{in} = 25\ °C$, with a drying gas flow rate of 11 L/min (recorded experimentally for a cake with a height of 50 mm) and an initial mass of solvent of 1.79 g. Both graphs include the outputs for different values of "f", including 1, 0.66, and 0.5. Figure 4 shows the solvent mass $M(t)$ versus time, where the drying rate was calculated from the gradient of these lines. This is to be compared to the drying rate measured experimentally during the constant drying rate period. Figure 5 shows the temperature of the cake and solvent, $T_s(t)$ versus time. As mentioned above, it is assumed that the exit gas stream, the cake particles, and the solvent are in thermal equilibrium. The temperature of the cake and solvent in the exiting gas at time t is assumed to be the same. The minimum temperature from this plot was compared with the minimum outlet temperature measured experimentally. The comparison of the drying model outputs with the experimental data is described in the following section.

5.2. Model Validation. The experiments shown in Figure 6 are selected from the DoE to validate the model. For clarity of the values used for the model inputs, the description of the experimental measurement used for each input of the model is shown in Table 2. It is important to note that the initial mass of the solvent used for the model is the solvent mass after the first 30 s of drying, that is, after the mechanical drying stage has occurred.

The temperature profiles are shown in Figure 6 for varying temperatures and pressures for a cake height of 50 mm. The "spikes" in temperature are due to the intermittent removal of the drying port for drying rate measurement. A preliminary control experiment was carried out without the intermittent removal of the port. The difference between the two profiles for the inlet temperature was within $\pm 1\ °C$. The minimum outlet temperature was 1.5 °C higher when carrying out intermittent weighing compared to without intermittent removal of the port. This therefore shows that it is a sound method for extracting the drying curve and measuring the outlet temperature.

The outlet temperature initially decreases at the start of drying, demonstrating the effect of the evaporative cooling.[17]

Table 2. Inputs to the Drying Model from Experimental Data

symbol	model input	experimental measurement
$\dot{V}_{in}(t)$	initial volumetric gas flow rate above the sample	average gas flow rate during drying, measured on the port inlet
P_{in}	pressure above the cake	inlet pressure set by the pressure regulator
P_{out}	pressure below the cake	average pressure measured on the outlet of the drying receiver vessel
$T_{in}(t)$	inlet temperature	average inlet temperature, measured during the time period where the drying rate is being measured, i.e., the constant rate drying period
$M(t)$	initial mass of solvent	mass of solvent as a function of time
T_e	temperature of the environment	average temperature of the lab

The outlet temperature tends to plateau at a minimum temperature, until a sudden increase occurs in the form of an inflection, indicated by the arrows in Figure 6.

The time of the outlet temperature inflection was compared with the time that the mass of the solvent reaches zero in the drying model, as shown in Figure 7. The time of this inflection correlates reasonably well with the time when the mass of solvent reaches zero in the model. The underestimation of the prediction is most likely because the model does not take into account the intermittent removal of the port during drying.

It is important to note that the time of this inflection may be affected by other factors at this stage of the drying, which involve processes that are very difficult to model realistically. Despite this, the detection of this time of inflection could potentially be a reasonable indication of when the sample has reached a suitable level of dryness. It is suggested that this may be useful for an online estimation of moisture content for a continuous drying process in the CFD.

The drying rate for samples that were dried under varying cake heights, inlet temperatures, and inlet pressure is shown in Figure 8. The error associated with the drying rate is ± 0.0015 g/s because of the limitations of the measurement technique and the difficulty in extraction of the gradient from the mass of cake vs. time plots.

It can be observed clearly that increasing the inlet pressure has a significant effect on increasing the drying rate. The pressure increases the flow rate of the drying gas, which is known to increase the drying rate.[18] Figure 8 also shows that the drying rate increases with inlet temperature and is more significant at higher pressures. Similar drying rates were measured for 20 and 50 mm cakes; however, the magnitude of the error bars associated with the measurement of the drying rate indicates that it is difficult to determine the difference in drying rate at varying cake heights.

The initial model, shown in red, predicts the drying rate reasonably well for the lower pressures. The prediction of the drying rate for the drying experiments carried out at 2 bar(g) is widely overestimated. It is suggested that this is because the model assumes that the outlet gas is saturated and does not consider this "nonsaturation" of the gas when the inlet pressure is increased.

The model was therefore modified to include a mass-transfer coefficient to capture this nonsaturation, as explained in the description of the drying model. Figure 9 shows that decreasing the value of f reduces the predicted drying rate, bringing it closer
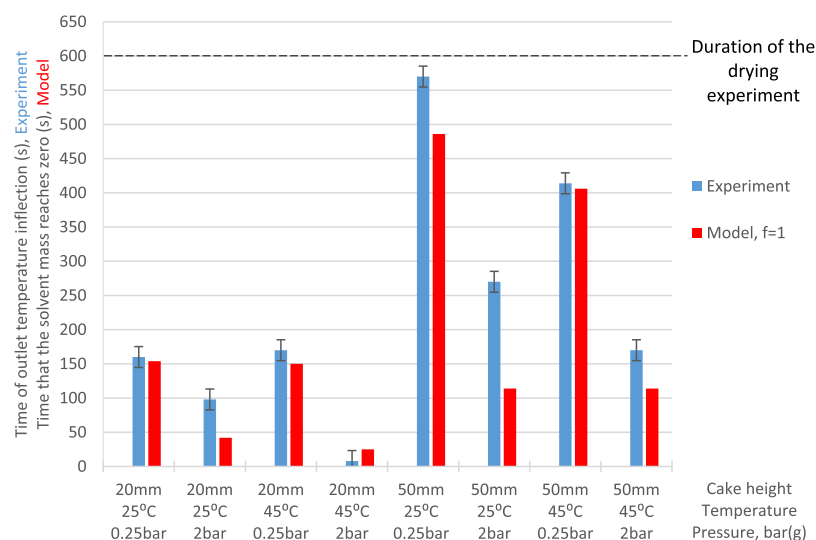
Figure 7. Time of outlet temperature inflection of sodium bicarbonate and water compared to drying model prediction of the time the mass of solvent reaches zero. Blue = drying rate measured experimentally; Red = original model ($f = 1$).
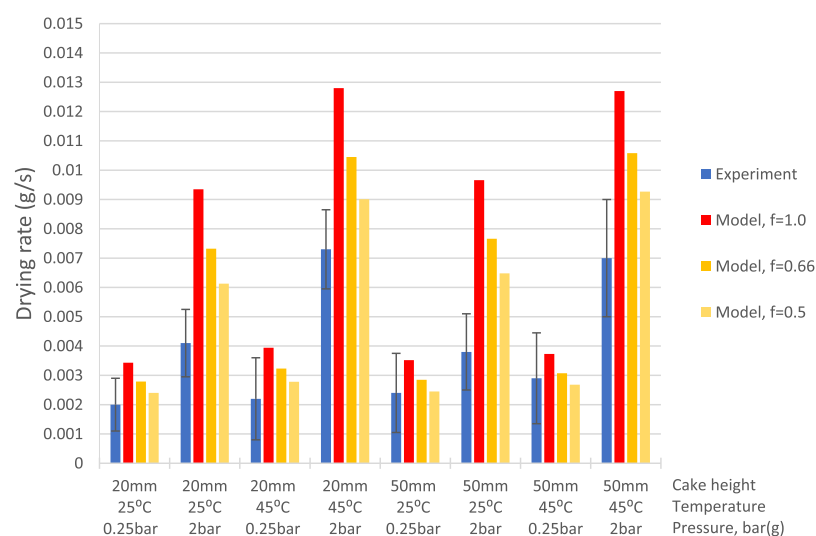

Figure 8. Drying rate of sodium bicarbonate and water compared to drying model prediction. Blue = drying rate measured experimentally; red = original model ($f = 1$); orange = ($f = 0.66$); and light orange = model ($f = 0.5$), where f is a factor incorporating the effect of nonsaturation of the outlet drying gas. f corresponds to the level of full saturation simulated by modeling.

to the drying rate measured experimentally, thereby improving the performance of the model at higher pressures.

The minimum outlet temperatures measured experimentally are compared to that predicted by the model in Figure 9. The experimental values for the outlet temperature follow the trend of what would be expected, increases with increasing inlet temperature and pressure.[19] The underestimation of the minimum outlet temperature predicted by the model is thought to be mainly due to the increase in temperature below the cake, occurring during the removal of the port for weight measurement during drying.

The inclusion of the f factor, for incorporating the nonsaturation of the exit gas, was used for the prediction of the minimum outlet temperature. The same values of "f" used for the drying rate predictions were used. Figure 9 shows that if the value of "f" is too low (e.g., f = 0.5), there is possibility of causing the predicted value of the outlet temperature to become overestimated. If this model is to be used to predict other drying model systems investigated with this drying rig, care must be

taken in choosing a suitable value of "f" so that the estimation of the nonsaturation is incorporated without reducing the model's performance.

5.3. Model Validation Experiments. The "corner points" of a DoE were used as the experiments that could be compared with the drying model. The results for the DoE "corner points" from the drying experiments with sodium bicarbonate are shown in Table 3.

The LOD at the end of each drying experiment is also shown in Table 3. However, the LOD after the 10 min of drying for most experiments was approximately 0.3−0.4%, apart from the experiments with the lowest inlet temperature and pressures. The moisture content of the raw sodium bicarbonate particles before they were wetted (before the experiment), that is, their original moisture content, was 0.3%. This confirms that, for the majority of experiments, the particles were dried to their original moisture content after 10 min of drying. There were two experiments where an LOD of 0.1% was achieved after 10 min of
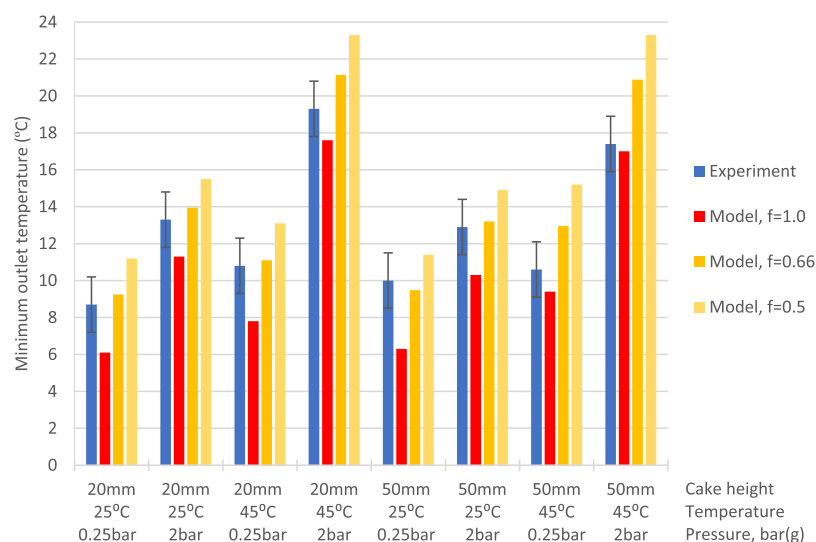
Figure 9. Minimum outlet temperature of the drying gas measured experimentally during the drying of sodium bicarbonate and water compared to drying model prediction. Blue = minimum outlet temperature measured experimentally; red = original model ($f = 1$); light orange = model ($f = 0.5$); and orange ($f = 0.66$), where f is a factor incorporating the effect of nonsaturation of the outlet drying gas. f corresponds to the level of full saturation simulated by modeling.

Table 3. Experimental Data of the Most Extreme Data Points of the DoE for the Sodium Bicarbonate Drying Experiments[a]

cake height (mm)	inlet temperature set point (°C)	inlet pressure (bar, g)	average drying gas flow rate (L/min), ±1 L/min	average outlet pressure (mbar, g), ±60 mbar, g	average temperature above the cake during constant drying rate period (°C), ±°C	solvent mass after 30 s (g) ±0.03 g	LOD (%) ±0.15% (%)	extent of agglomeration (%) ±4% (%)
20	25	+0.25	11	−500	23.6	0.57	2.0	17
20	25	+2	26	+480	23.8	0.41	0.4	38
20	45	+0.25	12	−470	29.1	0.63	0.4	12
20	45	+2	23	+410	39.1	0.33	0.4	8
50	25	+0.25	11	−505	24.5	1.79	0.9	52
50	25	+2	23	+215	24.6	1.16	0.3	42
50	45	+0.25	9	−545	38.1	1.58	0.4	20
50	45	+2	19	+75	44.1	1.47	0.3	57

[a]Comparison of the following measurements: average drying gas flow rate, average outlet pressure, average inlet temperature during constant drying rate period, solvent mass after 30 s of drying, LOD after 10 min of drying, and the extent of agglomeration.

Table 4. Extent of Agglomeration of Sodium Bicarbonate in Water; Photos Show the Agglomerates Retained on a 1 mm Sieve; Inlet Air Temperature Set Point for These Experiments Was 45 °C; Extent of Agglomeration Has an Experimental Error of ±4%

drying, showing that it is possible to obtain an even lower moisture content with this system.

The extent of agglomeration for each experiment used for the model validation is also shown in Table 3. A selection of the

extent of agglomeration experiments is also presented pictorially in Table 4.

In order to discuss the agglomeration of the cakes in these experiments, it is important to understand that the cake is wetted
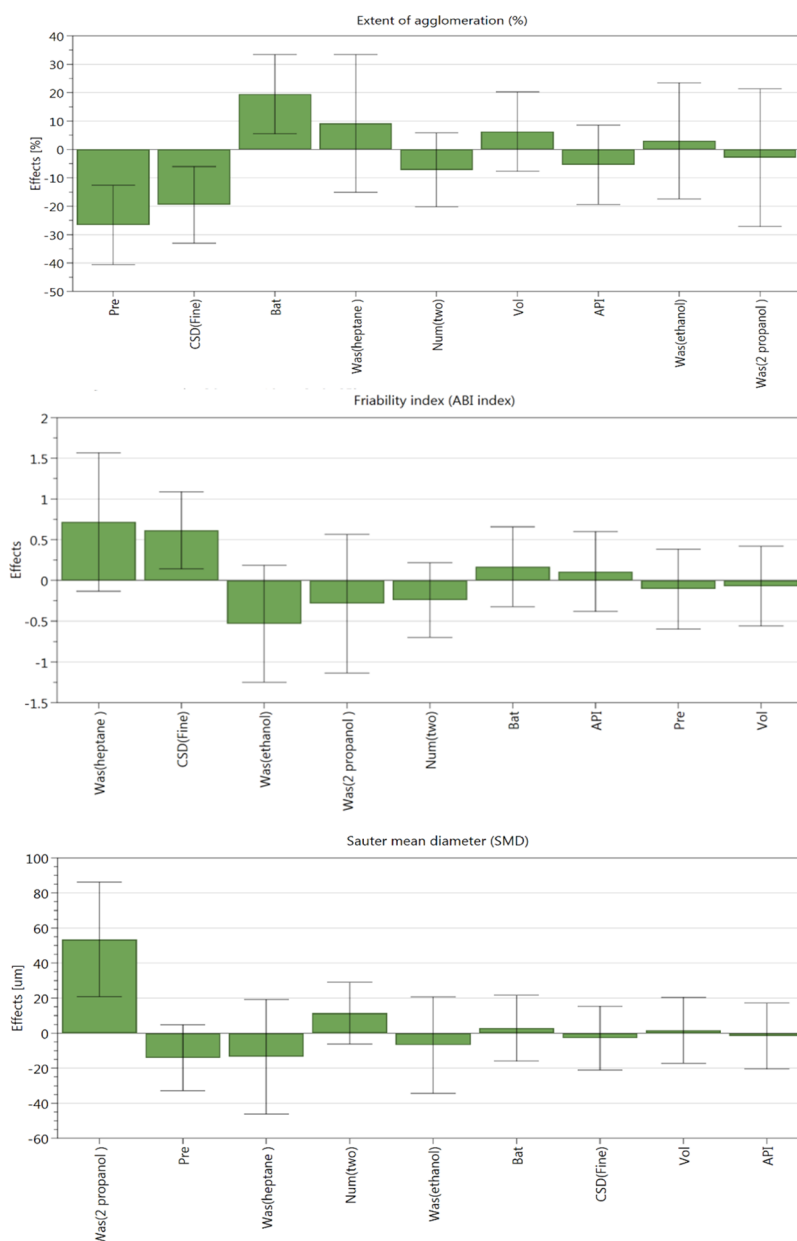
Figure 10. DoE factor effect plots on the extent of agglomeration ($R^2 = 0.81$), ABI index ($R^2 = 0.59$), SMD ($R^2 = 0.65$). The error bar expresses the 95% confidence interval that is related to the coefficient. Where the error bar is bigger than the effect of the considered factor, the analyzed response is considered null. For process factors, the values of the effects (computed as twice the MLR coefficients) are plotted sorted (in absolute value) in descending order. On the *x*-axes, the different factors showing a positive and negative effect are reported.

with a saturated solution of sodium bicarbonate in water, containing approximately 10% by mass of dissolved sodium bicarbonate. As the saturated solution is evaporated from within the pore structure of the cake, the sodium bicarbonate in the solution may form particle−particle bridges, thereby binding them together to form agglomerates.[20]

In Table 4, it is shown that there is a considerable increase in the extent of agglomeration when increasing the cake height from 20 to 50 mm. Increasing the cake height increases the resistance to flow,[21] lowering the flow rate of gas and thereby potentially decreasing the performance of drying. However, there are other factors that can influence agglomeration in this case, for example, the effectiveness of the mechanical removal of the solvent within the first few seconds of drying,[6] as well as cake compaction which can assist with binding particles together.[20,21]

The lowest extent of agglomeration displayed in Table 4 is for a 20 mm cake height, with an inlet pressure and temperature of 2 bar(g) and 45 °C, respectively. It is interesting that this is also the experiment with the lowest mass of solvent after the first 30 s. Table 3 shows that increasing the inlet pressure results in a lower mass of saturated solution left within the cake after the first 30 s of drying. Increasing the inlet pressure raises the flow rate of the drying gas, improving the performance of the initial mechanical removal of the saturated solution, reducing the amount of saturated solution left within the cake during the constant drying rate period, thereby potentially reducing the extent of agglomeration.[6] This suggests that increasing the inlet pressure can be effective in terms of preventing agglomeration by assisting with the mechanical removal of the saturated solution.

However, under other conditions, increasing the inlet pressure to 2 bar(g) may encourage agglomeration. For example, the highest extent of agglomeration displayed in Table 4 is for a 50 mm cake height, with an inlet pressure and temperature of 2 bar(g) and 45 °C. The result of this agglomeration measurement can be visualized in the photo in Table 4. The photo shows that a large amount of cake has bound into one large agglomerate. It is thought that in this case, the inlet pressure has been raised to a level where the cake may have been compressed. At the beginning of the drying experiments, when an inlet pressure of 2 bar(g) was applied while applying vacuum underneath, it was visually observed that the level of the cake was reduced by approximately 1−2 mm, suggesting that the cake was compressed. It is thought that if a section of the cake becomes compacted, the majority of the flow of the drying gas will bypass this compacted area, reducing drying performance in this region, which can result in large agglomerates being formed.[20,21]

These observations suggest that for a system where positive pressure is applied above the cake (controlled by a pressure regulator on the inlet of the system) and vacuum is applied beneath the cake, an optimum inlet pressure is required to achieve the best drying performance in terms of preventing agglomeration. The results displayed in Table 4 suggest that using an inlet pressure of 1 bar(g) can considerably reduce agglomeration, even when processing larger cake heights. This evidence is also backed up by the results of the DoE, as shown in the Supporting Information section. This suggests that an inlet pressure of 1 bar(g) in this system does not significantly compact the cake and assist with agglomeration but produces a flow rate which improves the performance of the initial mechanical removal of the saturated solution, thereby reducing agglomeration and improving the drying performance.

5.4. Application to Other Compounds. A PLS fitting model was used to determine the correlation between factors and responses. This fitting model is used in case several responses were measured and the model is used to simultaneously represent the variation of all the responses in response to the variation of the factors.

Figure 10 displays effect plots of predicted values of the selected responses, when the factor varies from its lowest to its highest level.

The effect plots and the experimental evidence observed during this work were used together to qualitatively define the parameters affecting agglomeration extent, the strength of agglomerates, and the propensity to modify PSD due to particle−particle aggregation.

The extent of agglomeration effect plot shows a good R^2 value (0.81), while friability index and SMDs show poor R^2 values (respectively 0.59 and 0.65). Therefore, these effect plots can be used to qualitative determine which isolation and material parameters may affect these responses.

From the extent of agglomeration effect plot, a positive correlation between the extent of agglomeration and water bath and hence drying gas temperature and wash solvent used can be observed. Increasing the bath temperature and therefore increasing the temperature of the nitrogen flowing into the cake during drying can facilitate agglomerate formation. This is correlated to the solubility of API in the residual solvent. Increasing the temperature of gas facilitates the particle surface dissolution and therefore increases the amount of API dissolved in the residual solvent trapped in the cake after washing, promoting agglomerate formation. For instance, considering the

experiment where the cake is wetted with IPA, the API solubility dependence[22] follows this trend: 0.124 g/g at 25 °C, 0.157 g/g at 40 °C, and 0.209 g/g at 55 °C. In the case of cake wetted instead with a nonsolvent, like *n*-heptane, the solubility dependence is much less strong: 0.0001 g/g at 25 °C, 0.0002 g/g at 40 °C, and 0.0003 g/g at 55 °C. A similar effect is observed for *n*-dodecane (0.0006 g/g at 25 °C, 0.0008 g/g at 40 °C, and 0.001 g/g at 55 °C). Therefore, the correlation with agglomeration propensity and gas temperature is much stronger in the case of solvent that exhibits high API solubility. DoE results related this effect and the correlation of it with LOD are reported in Supplementary Information. The correlation between agglomeration propensity and solvent properties is described in Supplementary Information.

A negative correlation between the extent of agglomeration and particle grade (paracetamol PSD), feed pressure, number of washes, and cake mass is observed. In general, smaller particles with broader PSD have higher propensities to form particle−particle bridges. As reported by Freire et al. (2014),[23] vapor and liquid diffusion into the cake is regulated by the cake tortuosity and cake porosity properties. When the cake is formed, the PSD plays a major part in defining tortuosity, which is an important contributor to the resistance to gas flow and hence gas velocity and the opportunity for the gas to contact the wet crystal surfaces and remove the residual solvent left from the washing process. This is the reason why the effect plot shows that powder paracetamol, with a much lower surface area than micronized paracetamol (specific surface area of powder paracetamol, 0.276 m^2/g, micronized paracetamol, 0.725 m^2/g),[b] has reduced agglomeration propensity during drying. Further description of this correlation with LOD is reported in Supplementary Information.

When increasing the feed pressure of the nitrogen drying gas while also applying vacuum on the bottom of the filtration/drying chamber, two mechanisms are promoted:

- Creation of a plug flow front of material (gas) that further deliquors the cake and reduces the initial solvent content
- Rise in solvent evaporation efficiency due to the reduction of the initial and constant drying period due to the constant flux of nonsaturated and heated gas that flows in the wet cake with improvement of the mass-transfer efficiency.

The inverse correlation between extent of agglomerate formed and the amount of washes done was explained by Ottoboni et al. (2019 and 2020).[4,13] A more detailed explanation and the correlation of this factor with LOD is described in Section 4.4.3.

Agglomeration after a general drying process can also be influenced by particle shape, initial moisture content (deliquoring efficiency), solvent properties, such as viscosity, presence of residual impurities or residual mother liquor, and agitation mechanism and speed.[22,24−27]

Note that by reducing the initial solvent content (by the deliquoring effect), the probability of bridging point formation between particles is reduced.[19]

The friability index (ABI index) effect plot cannot be used for quantitative evaluation because of the low R^2 value. As reported in Figure 10, the ABI index effect plot shows a low R^2 value: the method proposed by Birch and Marziano (2013)[6] and used in this paper is one of the few methods available to determine the strength of the agglomerates. Other techniques available require a larger quantity of samples than the quantities provided during

the drying experiments undertaken in this work.[7,22,28] None of the techniques described in the literature are able to provide a quantitative evaluation of the mechanical properties of the agglomerates. Furthermore, the analytical procedure used here is susceptible to operator error causing marginal variation in ABI index determination.

From this plot, a linear correlation between particle grade (PSD) can be observed.

The ABI index increases with increasing particle size of the material forming the cake, representing softer agglomerates that are easy to break. The micronized material usually formed hard agglomerates with a low ABI index, whereas the powder particles formed softer agglomerates with a higher ABI index.

Bath temperature negatively affected the friability index: increasing the bath temperature and therefore increasing the temperature of the nitrogen flowing through the cake during drying can facilitate strong agglomerate formation.

If the compound shows high solubility in the wash solvent selected, the amount of API molecules dissolved in the liquid phase will be high; during drying, the solvent evaporates depositing those molecules on the crystal surface causing particle size enlargement and interparticle bridge formation with the consequence of particle size increase.

A similar correlation factor response can be observed in the SMD effect plot.

As reported in the method section, washing was stopped at breakthrough. The susceptibility of particles to form agglomerates/increase the particle size and size distribution of the dried material can also be correlated with; the solvents propensity to evaporate, API solubility, solvent viscosity, and system wettability.

The effect of paracetamol grade, wash solvent used, number and volume of washes used, and the inlet gas temperature on the SMD of isolated particles, LOD during 30 min drying, friability index, and the extent of agglomeration of isolated particles is described using the 2D contour plots reported in the Supporting Information section. A detailed description of these correlations is reported in the Supporting Information section, while here a summary of the main results is reported.

In general, the higher the material surface area, correlated to the presence of smaller particles, the higher the tortuosity, and the higher the propensity to trap solvents in interparticle cavities. All factors which inhibit the flux of nitrogen through the cake thereby lower the drying rate, promoting agglomeration during drying.

To investigate the role of wash solvent nature on the final isolated material, four different wash solvents were selected: ethanol and IPA, showing high API solubility, and *n*-heptane and *n*-dodecane, showing really low API solubility.

The solubility of paracetamol in the wash solvents selected all, to varying degrees, affect the size of single particles by cementing them to form larger aggregates (particle–particle aggregation to form particles with size less than 1 mm) and to form large agglomerates (agglomerates bigger than 1 mm).

In general, the solubility of paracetamol in the different solvents is the main factor affecting particle aggregation and agglomeration:[22,26] indeed, the bigger SMD values and bigger extent of agglomeration with formation of harder agglomerates (lower friability index) are observed in the case of ethanol as a wash solvent and the smaller SMD values are obtained for *n*-dodecane.

By selecting a wash solvent exhibiting high API solubility, the dried material shows a high agglomeration propensity and the

agglomerates formed are hard and difficult to break with a consequent need for a milling downstream process to get the required particle size and size distribution for the formulation stage.

To design a washing process capable of removing completely the residual mother liquor trapped in the cake cavities, the decision related to how many washings and the volume of wash solvent used per each wash need to be considered. The residual crystallization solvent left in the cake after drying is responsible for particle cementation and consequently solvent entrapment between particle–particle cavities and the increase of residual solvent content after drying.

By increasing the number of washes, thereby increasing the amount of wash solvent, the extent of agglomeration is reduced with the formation of hard agglomerates bigger than 1 mm and the size of particle–particle aggregates is also reduced (smaller than 1 mm size).

However, in case the solubility of mother liquor and wash solvent used is drastically different, "antisolvent" effect[c] during washing occurs, promoting the API precipitation during the first wash causing particle–particle agglomeration during drying.

Washing the cake with small and repeated aliquots of wash solvent improved removal of residual mother liquor trapped in the cake without the possibility of back-mixing effects with a consequent increase of washing efficiency. However, as reported by Ruslim et al. (2007),[8] cake desaturation (filtration and washing to breakthrough) is responsible for washing efficiency reduction and increase of LOD compared to a similar washing process where washing is stopped to dryland. Therefore, it is recommended in order to enhance washing performance stop filtration at dryland and follow by a washing stage where a series of small aliquots of wash solvent are fed and displaced each to dryland (it is suggested that at least three to four washing steps are used).

The design of a convective drying process requires the selection of an appropriate gas inlet temperature. The gas inlet temperature mainly affects the propensity to form bigger agglomerates (bigger than 1 mm) and their strength: by increasing gas inlet temperature, softer agglomeration propensity is observed.

6. CONCLUSIONS

The experimental approach and its embodiment in the CFD have been demonstrated. The value of a DoE approach in planning laboratory investigation and subsequent data analysis to inform the modeling activities has been shown. The model has useful predictive capabilities and has been shown to be of value in shaping the design of the CFD and prediction of its processing capacity.

6.1. Model Validation Experiments. The results of the experimental data demonstrated the significance of the pressure of the inlet drying gas and its effect on the drying rate of the sodium bicarbonate particles. It was suggested that an inlet pressure of 1 bar is required for this system to obtain optimum drying performance. The future designs of the AWL continuous carousel filter dryer units may therefore allow for higher positive inlet pressure of the drying gas in order to gain optimum drying of the solid materials.

The drying model was able to make good predictions for the drying rate and minimum outlet temperature for low inlet pressures of 250 mbar. However, an alteration to the model was required to incorporate an estimation for the nonsaturation of

the exit gas thought to exist when using inlet pressures above 1 bar.

Interestingly, a temperature inflection in the outlet temperature was observed during the drying experiment. The time of this occurrence could be a reasonable indication for the time when the drying process has reached a suitable level of dryness. This could be incorporated into the AWL continuous filter dryer technology as a means of estimating the moisture content online and could therefore be useful for the control of continuous drying processes.

6.2. Application to Other Compounds. Paracetamol was selected as a test compound to evaluate the efficiency of the prototype for drying API and to test the efficiency of the system to maintain particle attributes during isolation.

The results presented in the DoE experiments show the key parameters responsible for particle agglomeration/aggregation during drying. Fewer and softer agglomerates were formed in the case of cakes made with large grade primary particles: reducing the cake surface area and tortuosity by using bigger particles, thereby reducing the probability of residual mother liquor becoming trapped in the cake pores with a consequent reduction of agglomerate propensity and improvement of drying rate. In case the cake is formed with small particles, the number of washes and the amount of wash solvent used need to be increased.

Solvent character represented by API solubility was another system parameter responsible for particle agglomeration/aggregation. Two different types of wash solvents were selected to evaluate the effect of API solubility on the responses studied: solvents showing high API solubility (ethanol and IPA), and solvents showing low API solubility (ethanol and IPA). In the presence of solvents that exhibit high API solubility, the API dissolved in the residual solvent gradually crystallizes on the particle surface because of solvent evaporation causing the formation of solid interparticle bridges and particle size enlargement. The residual ethanol (mother liquor) was mainly responsible for the single particle aggregation and agglomeration. To reduce the quantity of trapped mother liquor, it is therefore suggested to stop filtration at dryland, keeping the cake saturated with liquid, wash the cake with many, small aliquots of wash solvent with low API solubility (suggested *n*-heptane or *n*-dodecane) to prevent back-mixing effect, stop the final washing at breakthrough, and to apply a prolonged deliquoring to minimize the residual solvent content before drying (not commencing drying when the cake contains solvent that could be removed by drainage). To increase the drying rate and maximize drying of nonthermally sensitive API, such as paracetamol, it is suggested to increase the gas temperature to reduce the drying time to form softer agglomerates.

Overall, the equipment and approach have been demonstrated and the value of combining modeling and experimentation has been demonstrated ultimately in shaping the design of the AWL CFD.

ASSOCIATED CONTENT

Supporting Information

The Supporting Information is available free of charge at https://pubs.acs.org/doi/10.1021/acs.oprd.0c00035.

Material characteristics of the three paracetamol grades; cumulative distribution and distribution density of raw granular paracetamol; cumulative distribution and distribution density of raw micronized paracetamol;

cumulative distribution and distribution density of raw powder paracetamol; DOE chart populated by Minitab Software for the DoE (model validation), with experimental results; literature values of boiling point, enthalpy of vaporization, vapor pressure and liquid-phase heat capacity of the solvent used as wash solvents;[13−16] factors and responses for the DoE (model validation); measured and calculated flow rate of hot nitrogen in the four empty and filled ports in relation to the probe temperature and vacuum applied; corrected flow rate and mass of the cake during drying experiment where the four ports are filled with wet cake with solid mass of 4 g; temperature profile recorded by top, cake, and bottom probe during the drying experiment reported in Table S6 in port 2; DOE chart populated by Minitab Software for the DoE (model validation), with experimental results; extent of agglomeration of sodium bicarbonate versus inlet pressure and cake height; DOE chart populated by Minitab Software for the DoE (API experiments); DOE factors selected for the paracetamol screening experiments; paracetamol DoE responses; reproducibility plots of the SMD, LOD, ABI index, and extent of agglomeration of the different DoE experiments; effect of paracetamol grade on the different responses selected to evaluate the effect of drying on the final product; effect of paracetamol grade on the different responses selected to evaluate the effect of drying on the final product; effect of wash solvent characteristics on the different responses selected to evaluate the effect of drying on the final product; effect of wash solvent characteristics on the different responses selected to evaluate the effect of drying on the final product; effect of wash solvent characteristics on the different responses selected to evaluate the effect of drying on the final product; effect of number of washes on the different responses selected to evaluate the effect of drying on the final product; effect of number of washes on the different responses selected to evaluate the effect of drying on the final product; extra experiments to verify DoE trend (effect of number of washes); extent of agglomeration, friability index, and SMD of the three extra runs; effect of the amount of wash solvent used per each wash on the different responses selected to evaluate the effect of drying on the final product; effect of the amount of wash solvent used per each wash on the different responses selected to evaluate the effect of drying on the final product; extra experiments to verify DoE trend (effect of wash solvent quantity); extent of agglomeration, friability index, and SMD of the two extra runs; and effect of the amount of wash solvent used per each wash on the different responses selected to evaluate the effect of drying on the final product (PDF)

Additional Electronic Supporting Information is available free of charge at https://doi.org/10.15129/73200386-560e-41c5-846a-173db04f8cd0

AUTHOR INFORMATION

Corresponding Author

Sara Ottoboni − *EPSRC Centre for Innovative Manufacturing in Continuous Manufacturing and Crystallisation, University of Strathclyde, Glasgow G1 1RD, U.K.;* orcid.org/0000-0002-2792-3011; Phone: 01414447109; Email: sara.ottoboni@strath.ac.uk

Authors

Simon J. Coleman − *Department of Chemical & Process Engineering, University of Strathclyde, G1 1XQ Glasgow, U.K.; Alconbury Weston Ltd, Stoke-on-Trent ST4 3PE, U.K.*

Christopher Steven − *Department of Chemical & Process Engineering, University of Strathclyde, G1 1XQ Glasgow, U.K.; Alconbury Weston Ltd, Stoke-on-Trent ST4 3PE, U.K.*

Mariam Siddique − *EPSRC Centre for Innovative Manufacturing in Continuous Manufacturing and Crystallisation, University of Strathclyde, Glasgow G1 1RD, U.K.*

Marine Fraissinet − *Département de Genie Chimique-Genie des Procédes, UT Paul Sabatier, 31077 Toulouse, France*

Marion Joannes − *Département de Genie Chimique-Genie des Procédes, UT Paul Sabatier, 31077 Toulouse, France*

Audrey Laux − *Département de Genie Chimique-Genie des Procédes, UT Paul Sabatier, 31077 Toulouse, France*

Alastair Barton − *Alconbury Weston Ltd, Stoke-on-Trent ST4 3PE, U.K.*

Paul Firth − *Alconbury Weston Ltd, Stoke-on-Trent ST4 3PE, U.K.*

Chris J. Price − *EPSRC Centre for Innovative Manufacturing in Continuous Manufacturing and Crystallisation and Department of Chemical & Process Engineering, University of Strathclyde, Glasgow G1 1RD, U.K.*

Paul A. Mulheran − *Department of Chemical & Process Engineering, University of Strathclyde, G1 1XQ Glasgow, U.K.;* ⬡ orcid.org/0000-0002-9469-8010

Complete contact information is available at:
https://pubs.acs.org/10.1021/acs.oprd.0c00035

Author Contributions

All authors contributed with a specific focus as indicated: Ottoboni Sara, Coleman Simon, Price Chris, Siddique Mariam, Fraissinet Marine, Joannes Marion, and Laux Audrey for the experimental part; Barton Alastair and Firth Paul for the equipment design and fabrication; and Mulheran Paul, Coleman Simon, and Steven Christopher for the drying model and validation.

Notes

The authors declare no competing financial interest.

ABBREVIATIONS

EPSRC, Engineering and Physical Sciences Research Council; GMP, good manufacturing practice; API, active pharmaceutical ingredient; SMD, Sauter mean diameter; CMAC, continuous manufacturing and crystallization; GC, gas chromatography; IPA, isopropanol; NCE, new chemical entity; CFD, continuous filter drier; HMI, human machine interface; PSD, particle size distribution; DoE, design of experiment; LOD, loss on drying; CSD, crystal size distribution; *API, cake mass; Pre, nitrogen feed pressure; Vol, volume of wash solvent; Num, number of washes; Was, wash solvent; M, micronized paracetamol; F, powder paracetamol; AP2, Sauter mean diameter; So2, solvent content (LOD) after 30 min drying with drying rig; Dri, driving force after 5 min drying; Dri2, driving force after 15 min drying; Dri3, driving force after 30 min drying; Ca2, cake mass after 5 min drying; Ca3, cake mass after 15 min drying; Ca4, cake mass after 30 min drying; Fin, solvent content (LOD) after 30 min of drying with drying rig + overnight in fumehood; Fl, flow rate corrected after 5 min drying; Fl2, flow rate corrected after 15 min drying; Fl3, flow rate corrected after 30 min drying; (Fr), friability index (ABI index); % a, extent of agglomeration; Top, top temperature after 5 min drying; to2, top temperature after 15 min drying; to3, top temperature after 30 min drying; Bot, bottom temperature after 5 min drying; Bo2, bottom temperature after 15 min drying; Bo3, bottom temperature after 30 min drying; Ca5, cake mass before drying and after washing; Ini, initial temperature top; In2, initial temperature bottom; Hea, heat transfer in gas; He2, heat transfer in cake; Mea, mean delta temperature top-bottom; ABI, friability index also named agglomerate brittleness index,; iGC−SEA, inverse gas chromatography−surface energy analyzer; BET, Brunauer, Emmett, and Teller analysis to determine the surface area of particles.

ADDITIONAL NOTES

[a]The significance of the two filtration stopping conditions, dryland or breakthrough, arise from the tendency for cracks to form in filter cakes as a result of deliquoring. Halting the filtration at dryland ensures that the cake is fully saturated and makes cracking unlikely but retains impure mother liquor in all the interparticulate pores. Alternatively, breakthrough occurs when the cake is deliquored sufficiently for air or nitrogen from above the cake to form bubbles on the low pressure side of the medium supporting the cake. In this case, more of the impure mother liquor is removed but the cake is very likely to have cracks running all the way through the cake from top to bottom making subsequent washing much less effective.

[b]These values were calculated with the iGC−SEA, surface measurement systems. The BET method with octane vapor was used to calculate the specific surface area of the paracetamol grades.

[c]"Antisolvent" effects during washing is occurring when the addition of the wash solvent leads to a large reduction in solubility of the API and impurities during the washing step and can cause the precipitation of fine particles of API and impurities. To avoid antisolvent effect leading to dissolved API being precipitated during the first wash step, the first stage wash is recommended to be prepared using a mixture of pure crystallization and wash solvents.

REFERENCES

(1) McWilliams, J. C.; Allian, A. D.; Opalka, S. M.; May, S. A.; Journet, M.; Braden, T. M. The Evolving State of Continuous Processing in

Pharmaceutical API Manufacturing: A Survey of Pharmaceutical Companies and Contract Manufacturing Organizations. *Org. Process Res. Dev.* **2018**, *22*, 1143−1166.

(2) Ripperger, S.; Gösele, W.; Alt, C.; Loewe, T. Filtration, 1. Fundamentals. *Ullmann's Encyclopedia of Industrial Chemistry*; Wiley Online Library, Major Reference Works, 2013.

(3) Murugesan, S.; Sharma, P. K.; Tabora, J. E. *Design of Filtration and Drying Operations in Chemical Engineering in the Pharmaceutical Industry: R&D to Manufacturing*; Wiley: New York; 2010, pp 315−346.

(4) Ottoboni, S.; Price, C. J.; Steven, C.; Meehan, E.; Barton, A.; Firth, P.; Mitchell, A.; Tahir, F. Development of a novel continuous filtration unit for pharmaceutical process development and manufacturing. *J. Pharm. Sci.* **2019**, *108*, 372−381.

(5) U. S. Department of Health and Human Services, Food and Drug Administration, Center for Drug Evaluation and Research (CDER), Center for Biologics Evaluation and Research (CBER). *Q3D Elemental Impurities, Guidance for Industry*; ICH, 2015.

(6) Birch, M.; Marziano, I. Understanding and Avoidance of Agglomeration During Drying Processes: A Case Study. *Org. Process Res. Dev.* **2013**, *17*, 1359−1366.

(7) Papageorgiou, C. D.; Langston, M.; Hicks, F.; am Ende, D.; Martin, E.; Rothstein, S.; Salan, J.; Muir, R. Development of Screening Methodology for the Assessment of the Agglomeration Potential of APIs. *Org. Process Res. Dev.* **2016**, *20*, 1500−1508.

(8) Ruslim, F.; Nirschl, H.; Stahl, W.; Carvin, P. Optimization of the wash liquor flow rate to improve washing of pre-deliquored filter cake. *Chem. Eng. Sci.* **2007**, *62*, 3951−3961.

(9) Ottoboni, S. Developing strategies and equipment for continuous isolation of active pharmaceutical ingredients (APIs) by filtration, washing and drying. Ph.D. Thesis, Dept. of Chemical and Process Engineering, University of Strathclyde, Glasgow, U.K., 2018.

(10) Lim, H. L.; Hapgood, K. P.; Haig, B. Understanding and preventing agglomeration in a filter drying process. *Powder Technol.* **2012**, *300*, 146−156.

(11) Pubchem website. https://pubchem.ncbi.nlm.nih.gov/compound/23681127#section=Taste (accessed 14-11-2018).

(12) AWL website. www.a-w-l.co.uk (accessed 10-04-2019).

(13) Ottoboni, S.; Shahid, M.; Steven, C.; Coleman, S.; Meehan, E.; Barton, A.; Firth, P.; Sutherland, R.; Price, C. Developing a batch isolation procedure and running it in an automated semi-continuous unit: AWL CFD25 case study. *Org. Process Res. Dev.* **2020**, *24*, 520. , Just Accepted Manuscript

(14) MODDE software. https://umetrics.com/product/modde (accessed 22-05-2018).

(15) Triefenbach, F. Design of Experiments: The D-Optimal Approach and Its Implementation As a Computer Algorithm, Bachelor Thesis, Umeå University, Sweden, 2008.

(16) Eriksson, L.; Johansson, E. Multivariate Design and modelling in QSAR. *Chemom. Intell. Lab. Syst.* **1996**, *34*, 1−19.

(17) Adamson, J.; Faiber, N.; Gottlieb, A.; Hamsmith, L.; Hicks, F.; Mitchell, C.; Mittal, B.; Mukai, K.; Papageorgiou, C. D. Development of Suitable Plant-Scale Drying Conditions That Prevent API Agglomeration and Dehydration. *Org. Process Res. Dev.* **2015**, *20*, 51−58.

(18) Morris, K. R.; Nail, S. L.; Peck, G. E.; Byrn, S. R.; Griesser, U. J.; Stowell, J. G.; Hwang, S.-J.; Park, K. Advances in pharmaceutical materials and processing. *Pharm. Sci. Technol. Today* **1998**, *1*, 235−245.

(19) Lamberto, D. J.; Diaz-Santana, A.; Zhou, G. Form Conversion and Solvent Entrapment during API Drying. *Org. Process Res. Dev.* **2017**, *21*, 1828−1834.

(20) Tsosas, E.; Metzger, T.; Gnielinski, V.; Schundler, E. *Ulmann's Encyclopedia of Industrial Chemistry*, 11th ed.; Wiley-VCH; Weinheim, 2012.

(21) Ottoboni, S.; Simurda, M.; Wilson, S.; Irvine, A.; Ramsay, F.; Price, C. J. Understanding effect of filtration and washing on dried product: paracetamol case study. *Powder Technol.* **2020**, *366*, 305−323.

(22) Tamrakar, A.; Gunadi, A.; Piccione, P. M.; Ramachandran, R. Dynamic agglomeration profiling during the drying phase in an agitated filter dyer: Parametric investigation and regime map studies. *Powder Technol.* **2016**, *303*, 109−123.

(23) Freire, J. T.; Freire, F. B.; Perazzini, H. On the Influence of Particles Characteristics on Moisture Diffusivity during Drying of Granular Porous Media. *Adv. Chem. Eng. Sci.* **2014**, *04*, 7−16.

(24) Lekhal, A.; Girard, K. P.; Brown, M. A.; Kiang, S.; Khinast, J. G.; Glasser, B. J. The effect of agitated drying on the morphology of l-threonine (needle-like) crystals. *Int. J. Pharm.* **2004**, *270*, 263−277.

(25) Lekhal, A.; Girard, K. P.; Brown, M. A.; Kiang, S.; Glasser, B. J.; Khinast, J. G. Impact of agitated drying on crystal morphology: KCl−water system. *Powder Technol.* **2003**, *132*, 119−130.

(26) Kougoulos, E.; Chadwick, C. E.; Ticehurst, M. D. Impact of agitated drying on the powder properties of an active pharmaceutical ingredient. *Powder Technol.* **2011**, *210*, 308−314.

(27) Lamberto, D. J.; Cohen, B.; Marencic, J.; Miranda, C.; Petrova, R.; Sierra, L. Laboratory methods for assessing API sensitivity to mechanical stress during agitated drying. *Chem. Eng. Sci.* **2011**, *66*, 3868−3875.

(28) Zhang, S.; Lamberto, D. J. Development of New Laboratory Tools for Assessment of Granulation Behavior During Bulk Active Pharmaceutical Ingredient Drying. *J. Pharm. Sci.* **2014**, *103*, 152−160.